

RESEARCH

Open Access



Cytological and ultrastructural investigation of pathogen infection pathway and host responses in asparagus stem infected by *Phomopsis asparagi*

Liping Sun^{1,2}, Yange Li¹, Xiaoting Li¹, Xinyi Ruan¹, Yueyan Zhao¹, Ruidong Wen¹, Shuaijie Wei¹, Ning Chen¹, Yulan Zhang¹, Shufen Li^{1*} and Wujun Gao^{1*}

Abstract

Asparagus stem blight, a highly destructive disease in global asparagus cultivation, is caused by the fungus *Phomopsis asparagi*. However, the underlying mechanisms of the infectious process and pathogenesis of *P. asparagi* remain poorly understood. This study aims to elucidate the infection event of *P. asparagi* at the cytological and ultrastructural levels in asparagus stem through a microscopic observation. The host responses were also examined by microscopic observation and fluorescent probe. It revealed that *P. asparagi* germinated at either the tip or the middle of the conidia to produce short germ tubes on the surfaces of the asparagus stem at 20 h post-inoculation (hpi). The germ tubes penetrated the host cell wall with appressorium-like structures or narrow pegs at 1 day post-inoculation (dpi). At 3–5 dpi, a large number of *P. asparagi* hyphae colonized the epidermal cells. The hyphae were found to grow both intracellularly and intercellularly. The movement of hyphae between cells was facilitated by constricted invasive hyphae pegs. The hyphae exhibited bidirectional intracellular growth, extending and branching along the inner side of the cell wall within the stem cortex and towards the central cylinder. The fungal colonization resulted in cellular damage in plants, which is characterized by plasmolysis, rupture of the cell wall, and disruption of the cytoplasm. At 11 dpi, the fungi penetrated the parenchyma cells, and the fungal pycnidia were formed. At 13 dpi, the fungi penetrated the stem center parenchyma cell, where the conidia were released. In addition, the host defense response was investigated, which revealed a notably reduced germination rate of conidium, the formation of callose analogs, and the reactive oxygen burst. These findings provide unexpected perspectives on the infection process and host response in *P. asparagi*-plant interaction.

Keywords Asparagus stem blight, Host response, Infectious process, *Phomopsis asparagi*

Background

Asparagus (*Asparagus officinalis* L.), a perennial and dioecious species with a long lifespan, has been cultivated for over 2500 years and holds significantly economic value. It is widely recognized as the “king of vegetables” in the international market due to its rich nutrition and numerous health benefits, including anti-oxidant, anti-inflammatory, and anti-hepatotoxic properties (Yang et al. 2020). The occurrence of asparagus stem

*Correspondence:

Shufen Li

lishufen83@163.com

Wujun Gao

gaowujun@htu.cn

¹ College of Life Sciences, Henan Normal University, Xinxiang 453007, China

² School of Biological Engineering, Xinxiang University, Xinxiang 453007, China



© The Author(s) 2024. **Open Access** This article is licensed under a Creative Commons Attribution 4.0 International License, which permits use, sharing, adaptation, distribution and reproduction in any medium or format, as long as you give appropriate credit to the original author(s) and the source, provide a link to the Creative Commons licence, and indicate if changes were made. The images or other third party material in this article are included in the article's Creative Commons licence, unless indicated otherwise in a credit line to the material. If material is not included in the article's Creative Commons licence and your intended use is not permitted by statutory regulation or exceeds the permitted use, you will need to obtain permission directly from the copyright holder. To view a copy of this licence, visit <http://creativecommons.org/licenses/by/4.0/>.

blight caused by *Phomopsis asparagi* (Sacc), commonly referred to as the “cancer” of asparagus, has a severe impact on both yield and quality (Yang et al. 2012). This disease is prevalent in asparagus-producing regions, such as Asia, North America, Africa, Europe, and Southern Australia (Davis 2001; McKirdy et al. 2002; Elena 2006; Yang et al. 2012; Iwato et al. 2014; Zaw et al. 2017; Thao and Dung 2019), with more severe epidemics in Asian countries. China is the leading producer of asparagus in the world, but it faces a significant threaten of stem blight now, which is hampering the sustainable development of asparagus production (Zhang and Araki 2017). In particular, during the nutritional growth period of asparagus, warm and humid weather is more prone to facilitating the disease outbreak. In worst cases, if the plants were infected at very early stage, the disease would progress throughout the growing season and would cause yield loss up to 100% (Elena et al. 2006).

Previous studies have demonstrated that the causal pathogen responsible for asparagus stem blight is a hemibiotrophic filamentous fungus, which mainly damages young stems with occasional infections on branches and leaves (Uecker and Johnson 1991). The initial manifestation of the fungus is the development of small lesions or spots on the surface of the asparagus stem. These lesions progressively expand and produce yellow-brown spindle-shaped spots (Sonoda et al. 1997). Pycnidia, usually appearing at the core of a spot, serves as a secondary source of infection. The infected stems often die rapidly, ranking it as a more devastating pathogen over other asparagus diseases. Control measures of this pathogen include the application of fungicide and the implementation of cultivation practices. Yet, the complete eradication of this disease remains challenging (Takeuchi et al. 2018). Meanwhile, the potential risk of fungicide resistance evolved in the fungi over time and the increasing environmental pollutions pose limitations on their use. Thus, a more feasible strategy is to breed new asparagus varieties with high disease resistance.

The understanding of *P. asparagi*'s infection process is essential for breeding plans and disease managements. Additionally, this research can also help us to understand the interaction mechanisms between *P. asparagi* and asparagus. Following the development of modern microscopy techniques, the infection process for certain pathogenic fungi has been widely studied, such as *Magnaporthe oryzae* which causes rice blast, and *Fusarium graminearum* which is responsible for wheat scab, and *Verticillium dahlia* kleb, which is the causal agent of Verticillium wilt. The hemibiotrophic fungus *M. oryzae*, as a model fungus pathogen, has been extensively studied at cytological level. This fungus deploys a penetration peg to pierce the surface of the host plants (Howard and

Valent 1996; Talbot 2003). Once reaching the lumen of the tissues, the penetration peg would expand, forming the slender filamentous primary hypha. The peg serves as a conduit for the transportation of the nucleus and cytoplasmic contents from the spores into the primary hypha. The primary hyphae then undergo differentiation, which finally develops to the thicker and bulbous invasive hyphae. These invasive hyphae proceed and occupy the first invaded cells and then they invade the adjacent cells through plasmodesmata (Kankanala et al. 2007).

Upon infection of a pathogen, host cells undergo the formation of mastoid structures, callose deposition, and programmed cell death as a defense mechanism to impede or hinder pathogen invasion (Van Baarlen et al. 2004; Yin et al. 2017; Fincher 2020). In response to pathogen attacks, plants produce pathogenesis-related (PR) proteins, some of which are enzymes that degrade chitin and the (1,3)- and (1,3;1,6)- β -glucans of the fungal cell wall (Roulin et al. 1997; Kasprzewska 2003). Overexpression of these hydrolytic enzymes proved to be successful in enhancing the resistance of crops (Ali et al. 2018; Moosa et al. 2018). The oxidative burst represents an early reaction of plant tissues to pathogenic fungi, leading to swift production and release of Reactive Oxygen Species (ROS). These ROS include superoxide (O_2^-), hydroxyl radical ($OH\cdot$), and hydrogen peroxide (H_2O_2) (Wojtaszek 1997; Bolwell 1999). Both O_2^- and $OH\cdot$ exhibit high activity with dismutation to H_2O_2 . H_2O_2 is relatively stable and can be detected (Wojtaszek 1997). ROS has been proposed with antimicrobial properties and to play a role in intercellular communication (Fichman et al. 2023).

Previous researches primarily concentrated on the biological characteristics and control measures of *P. asparagi*. It is largely unknown for the infection pathway and the interaction of *P. asparagi* with plants.

In this study, we used a combination of microscopy techniques, including confocal laser scanning microscope (CLSM), scanning electron microscopy (SEM), and transmission electron microscope (TEM), to investigate the infection process, infection structures, and cell-to-cell movement of *P. asparagi*. Furthermore, the host responses, including callose accumulation and H_2O_2 production and distribution, were also examined using TEM and fluorescent probe method. The findings unravel the pathogenicity of *P. asparagi* and may be helpful for the disease control.

Results

Isolation and identification of the causal pathogen

The causal pathogen was isolated from a diseased asparagus stem which exhibited typical symptoms of stem blight (Fig. 1). To identify the isolated pathogen,

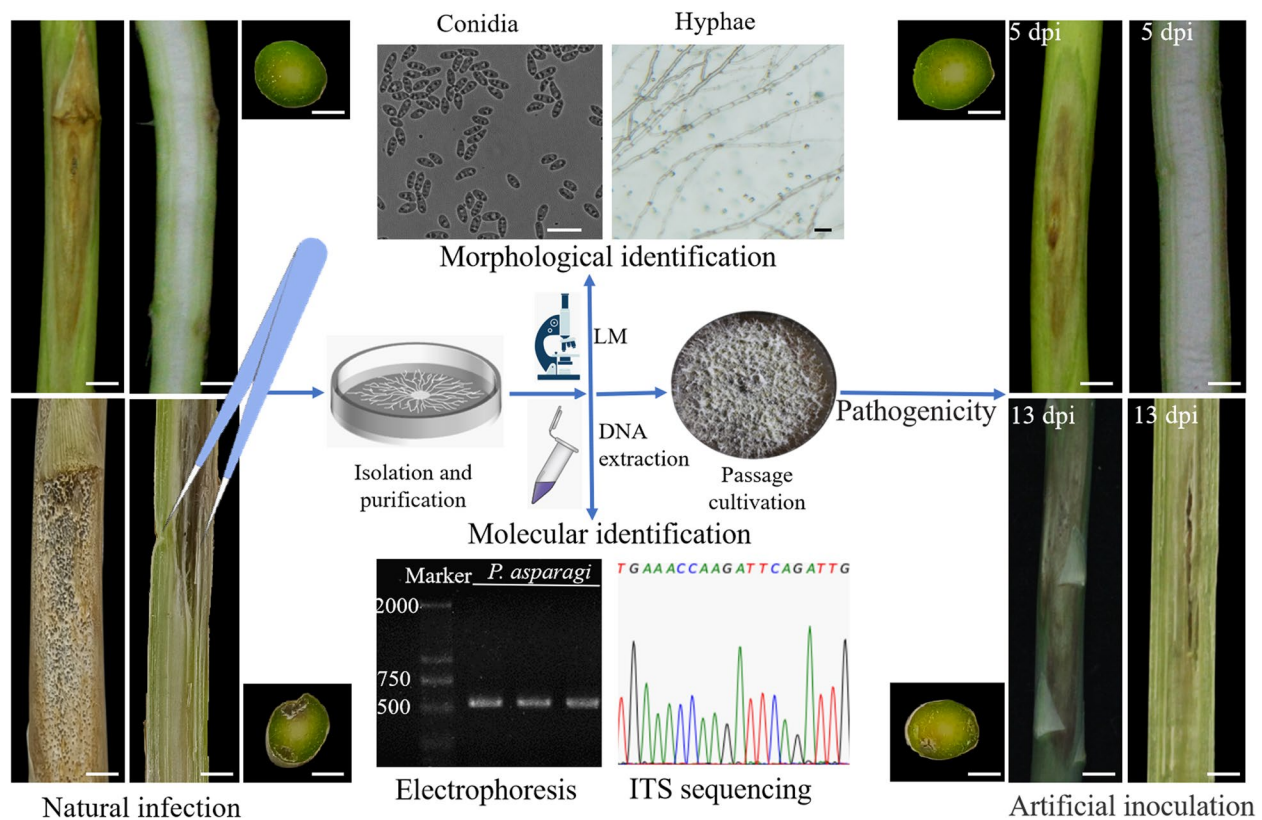


Fig. 1 The isolation and identification of the causal pathogen of asparagus stem blight. A diseased stem is cleaned and sterilized, then a sterilized knife is used to cut the stem longitudinally, and take a small area of diseased tissue culturing on potato sucrose agar (PSA) medium, followed by the subculturing purification. The identity of the causal pathogen includes the characteristics in medium and conidia, hyphae morphological, molecular identification, and pathogenicity assay

we employed the methods of morphology examination, rDNA ITS analysis, and a pathogenicity test. Initially, the mycelia of this pathogen display a fluffy white shape on the medium and then they turned grayish-white to yellowish-green. Within the black sporodochium, the pycnidia were formed either singly or in aggregates. The aerial hypha with the septum produced a short or long lateral branch. The conidia sizes are 1.8–3.3 $\mu\text{m} \times$ 6.0–8.8 μm , oblong or spindle-shaped, unicellular, colorless, with 1–2 oil droplets at each end. The ITS regions were PCR-amplified, which produced a fragment approximately 600 bp. A sequence comparison showed that the ITS shared a 99% sequence identity with that of *P. asparagi*. The pathogenicity was examined by inoculating asparagus stems. The infected stems all displayed typical stem blight symptoms, being consistent with the field disease symptom. These results were consistent with previous reports (Uecker and Johnson 1991; Yang et al. 2012; Zheng et al. 2015), and the pathogen was identified as *Phomopsis asparagi* (Sacc) (NCBI No: JQ614007.1).

Infection process and the appearance of *P. asparagi* on the asparagus stem surface

The infection process of *P. asparagi* on asparagus stems was observed at a series of time points by SEM. The results showed that the conidia adhered to the stem surface, and only about 8% of conidia germinated at 20 hpi (Fig. 2a). Each conidium produced a single or multiple germ tubes from one end, two ends, or the middle of the conidium (Fig. 2b–d). At 1 dpi, germ tubes invaded the epidermal layer by forming an appressorium with an enlarged tip (Fig. 2b, c); however, some of them became tapered and invaded the epidermal cells (Fig. 2d). Most developing germ tubes did not immediately infect host tissues but instead, they developed to runner hyphae. The runner hyphae produced multiple morphological appressorium-like structures, such as bifurcate appressorium (Fig. 2e–h), foot appressorium (Fig. 2i), and irregular appressorium (Fig. 2e). The terminus of the germ tube was swollen and differentiated into spherical appressoria (Fig. 2e, g). Some had an obvious infection peg at the front of the appressorium (Fig. 2g), while others did not

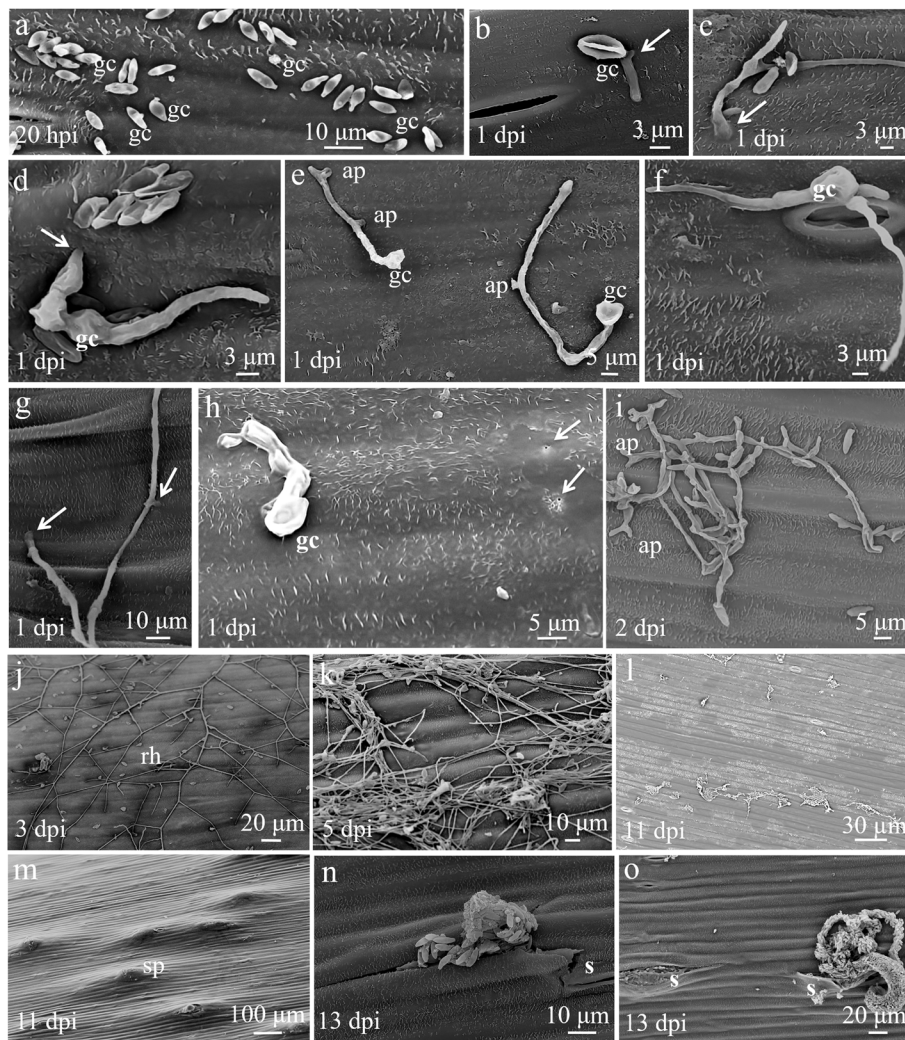


Fig. 2 The infection process and appearance of *P. asparagi* on asparagus stems. **a** The conidia germinated with a germ tube emerging from one end or middle of the conidium on the asparagus stem at 20 hpi. **b** A conidium germinated two germ tubes, and one germ tube invaded with an enlarged tip (arrowhead). **c** A conidium germinated three germ tubes, and one germ tube invaded with an enlarged tip (arrowhead). **d** The tip of one germ tube tapered and invaded the host cell surface (arrowhead). **e, g, h, and i** Various infection structures were formed. **f** The germ tube bypassed the opening stomata. **h** Penetration pores (arrowheads). **j and k** The hyphae network at 3 dpi and 5 dpi. **l** Residual hyphae net (11 dpi). **m** Sporodochium was formed underneath the epidermis. **n and o** New conidia were released through a stoma or surface. gc, germinated conidium; gt, germ tubes; rh, runner hyphae; s, stomata; ap, appressorium; sp, sporodochium; c, conidium

form an infection peg (Fig. 2e). Interestingly, *P. asparagi* may not enter host tissue by stomata as do many other fungi, even when they were in close contact with them (Fig. 1f). Penetration pores of about 0.5 μm in diameter were visible where hyphae were detached from the surface of the cell wall (Fig. 2h), indicating that the penetration peg was markedly constricted. The appressorium and hyphae were surrounded by gelatinous materials that may help them adhere to the stem surface (Fig. 2c, f–h). The runner hyphae grew and branched radially on stem surfaces or grew beneath the epidermis, forming hyphal nets at 3 dpi (Fig. 2j–l). No hyphal nets were found on

the host surface after 5 day of inoculation. At the later stage of the infection (at about 11 dpi), many humps-like sporodochia were observed (Fig. 2m). Finally, the epidermal layer were ruptured and a large number of conidia were released at around 13 dpi (Fig. 2n, o), in which the *P. asparagi* completed its life cycle.

The dynamics of fungal colonization in host tissues

In order to reveal the detailed colonization process, typical disease progression was observed. The hyphae inside the host stem were monitored at 1, 2, 3, 5, 7, 9, 11, and 13

dpi via CLSM, using WGA-AF488/PI to show the fungal infection dynamics.

There were no conspicuous symptoms at the inoculation site up to 2 dpi. The microscopic observations revealed that, at 1 dpi, *P. asparagi* could successfully penetrate asparagus stems, which is consistent with the results of SEM. At 2 dpi, the fungal hyphae grew inside the stem and invaded the adjacent cells. At 3 dpi, small light brown lesions were visible at the inoculation sites, and a large number of *P. asparagi* hyphae colonized the epidermal cells. At 5 dpi, necrosis was seen at the center of the lesion, and the hyphae suffused the epidermis and sclerenchyma layers, indicating a well-established necrotrophic phase (Fig. 3a). The statistical analysis showed that the disease indexes were at level 3 or below, and the lesion area was below 60% at 1–5 dpi (Fig. 3b, c). Then, the lesions continued to expand, forming yellowish-brown and spindle-shaped lesions. Notably, majority

of the lesions merged at 7 to 9 dpi (Fig. 3a). The disease indexes reached the highest level 5, and the lesion almost covered the entire stem (Fig. 3b). Additionally, the fungal hyphae rapidly expanded towards the central medulla (Fig. 3a–c). At 11 dpi, the stem wilt was visually apparent. The pycnidium formed a papillary orifice and appeared at the central part of the lesions. The hyphae reached the parenchyma cell and grew towards the central cylinder (Fig. 3a). The ratio of fungi hyphae was up to 80% (Fig. 3d). At 13 dpi, the stem was completely invaded. Laser confocal imaging showed that *P. asparagi* reached the stem center parenchyma cells and full-filled the cells with hyphae (Fig. 3a, d).

P. asparagi colonize inside of host tissues

To further investigate the *P. asparagi* colonization and proliferation in host tissues, we used CLSM and SEM to observe transverse sections of *P. asparagi*-infected

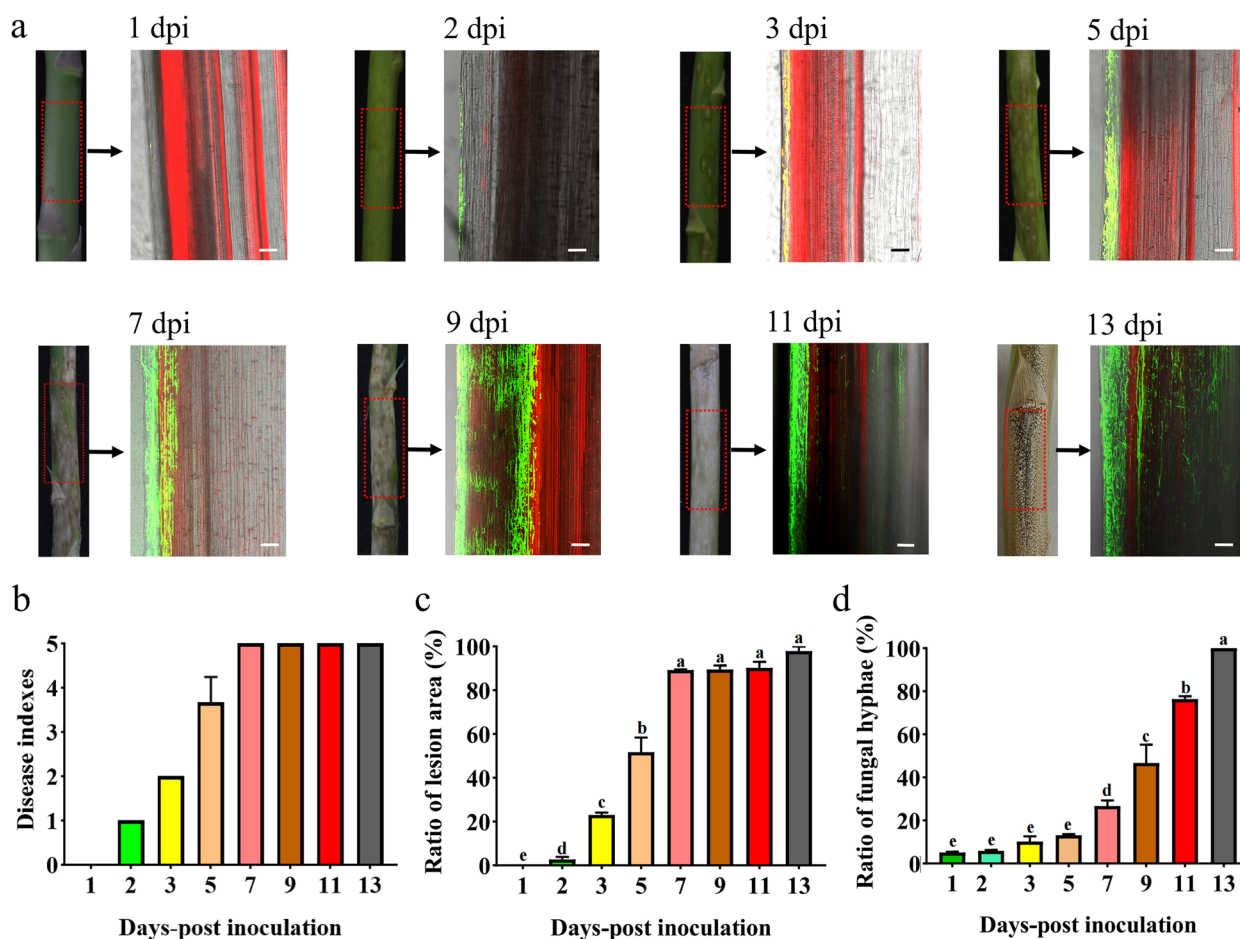


Fig. 3 The microscopic characterization of hyphae colonization in asparagus stems. **a** The red box indicates the sampling points on the stems. Fungal cells were stained with WGA-AF488 (green), and the plant cell wall was stained with PI (red). Scale bars: 100 μ m. **b**, **c**, and **d** The disease indexes, the ratio of the lesion area, and the ratio of fungal hyphae at eight-time points after fungi inoculation. Data from three biological replicates were analyzed by one-way ANOVA. Different letters indicate statistically significant differences ($P \leq 0.01$)

stems at 11 dpi. The CLSM results showed that hyphae spread over the whole cortical tissues and parenchyma cells of the stems, whereas only few hyphae were detected in vascular tissues. The pathogen hyphae were observed in the parenchymal tissues (Fig. 4a). Strikingly, the intercellular hyphae were thick and solid with a diameter of about 3–5 μm , which was similar to that in vitro culture medium and about three times to the diameter of intracellular hyphae (1–2 μm) (Fig. 4b, c). The hyphae ramified and became swollen when they breached the cell wall (Fig. 4d). In a longitudinal section at 11 dpi, pathogen hyphae were found expanding beneath the epidermis of host cells, where they formed pycnidia. Importantly, the cells in the epidermis regions were not positive by PI staining, indicating that the hyphae had lost membrane integrity (Fig. 4e, f), which agrees with their necrotic appearance.

Cell-to-cell movement of *P. asparagi* inside the asparagus stem

Through an extensive CLSM observation for cell-to-cell movement of *P. asparagi*, we observed that the hyphae had a slightly swollen end and experienced extreme constriction during penetration of the cell walls. Once they traversed, the pegs expanded to form the filamentous hyphae in the newly invaded cells with normal size, followed by the rapid proliferation within the cell (Fig. 5a–d, e–h). The intracellular growth of the hyphae was bidirectional, with growth and ramification along the inner side of the cell wall within the stem cortex, and grew towards the central cylinder (Fig. 5i, j, k).

Host subcellular changes of *P. asparagi*-infected stems

The TEM observations showed that the healthy cells had normal sub-cellular structure (Fig. 6a). However, in the infected tissues, the cytoplasm of host cells was coagulated, and the dark deposits were found to surround the

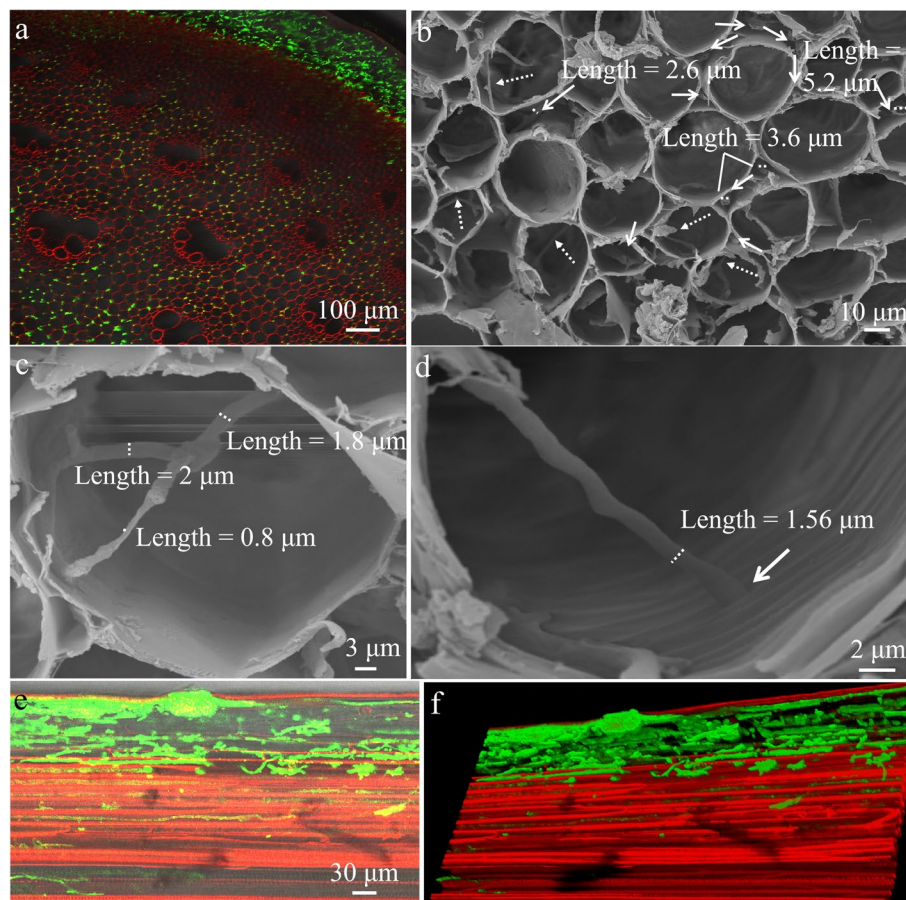


Fig. 4 *P. asparagi* colonization and expansion patterns in host tissues. **a** Hyphae distribution in the tissue. **b** Intercellular (solid arrow) and intracellular (dotted arrow) hyphae. **c** Intracellular hypha branching and morphological changes. **d** Hypha became swollen upon contacting with the cell wall. **e** Pycnidium was formed underneath the epidermis. **f** 3D reconstruction was obtained from 18 optical sections acquired with a z-interval of 1.5 μm

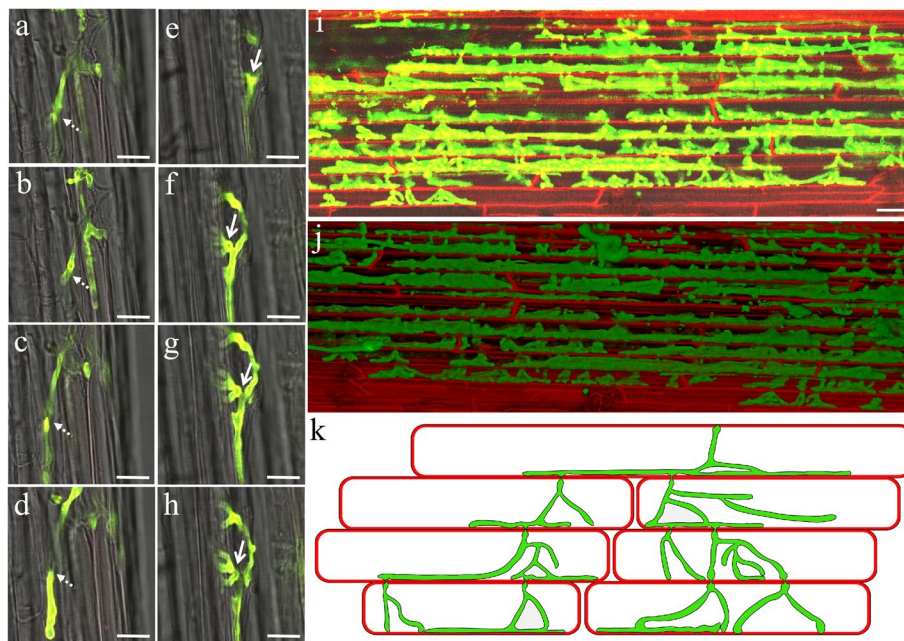


Fig. 5 *P. asparagi* proliferation and cell-to-cell movement. **a–d** and **e–h** The dynamic process of invasive hyphae tip swelled and then crossed the cell wall, followed by branching growth. **a–d** and **e–h** were layer scanning photos of the same sites, respectively. Arrows indicate the site of hyphae penetration. **i** Hyphae constriction during penetration. **j** 3D reconstruction is obtained from 39 optical sections with a z-interval of 1.5 μm . **k** A proposed model depicting *P. asparagi* proliferation and cell-to-cell movement. Scale bars: 10 μm

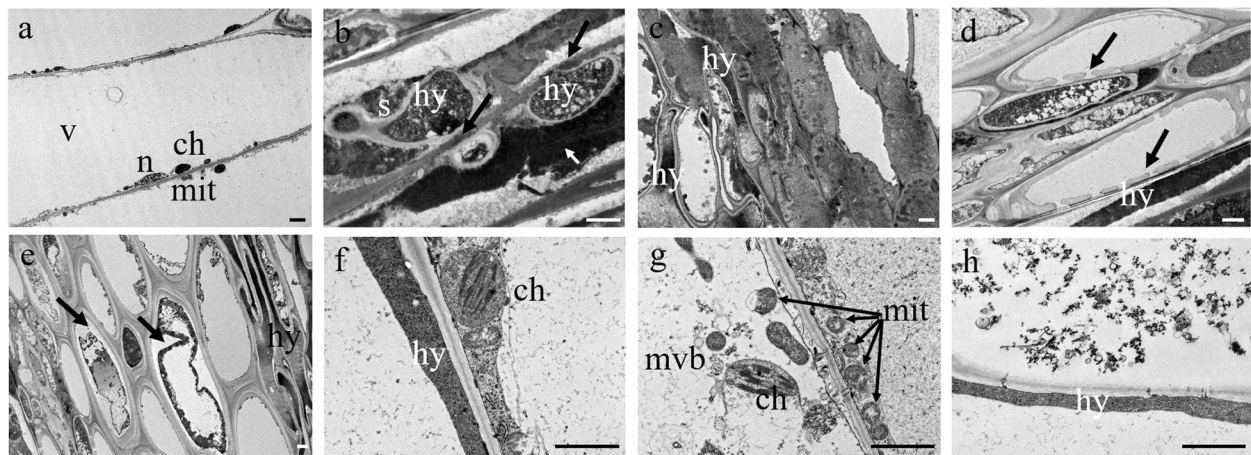


Fig. 6 Ultrastructure of the healthy and *P. asparagi*-infected stems at 3 dpi. **a** Healthy cells containing intact chloroplasts, mitochondria, nuclei, and large vacuoles. **b** Callose-like substance were deposited (black arrow) and dark deposits surrounded the hyphae (white arrow). **c** The cytoplasmic matrix of infected adjacent cells were more electron-dense. **d** Host cell wall was degraded (black arrow). **e** Plasmolysis of the infected cells (black arrow). **f** Chloroplasts were swollen. **g** Structural variations of chloroplast, mitochondrion, and multivesicular body. **h** Collapse of the infected host cells. n, nucleus, ch, chloroplasts, mit, mitochondria, v, vacuoles, hy, hyphae, s, septum, miv, multivesicular body. Scale bars: 2 μm

hyphal cell walls, resulting in ambiguity of organelles. The cell wall contacting hyphae became darker, probably because of callose-like material deposition, which may restrict the hyphae extension (Fig. 6b). Additionally, the cytoplasmic matrix of adjacent infected host cells became more electron-dense (Fig. 6c). The host cell

wall close to the hyphae was partially digested (Fig. 6d). Cell membrane contraction led to plasmolysis, and the electron density of protoplasm was increased (Fig. 6e). The chloroplasts in the host cell were swollen and less dense (Fig. 6f). The host cytoplasm and organelles, such as chloroplasts, were degenerated, and mitochondrial

cristae were blurry, granulated, locally vacuolized, and multivesicular bodies were formed (Fig. 6g). The collapse host cells were plasmolysized, which further impaired the cell membrane, leading to the cytoplasm cracking into lumps (Fig. 6h).

The responses of asparagus to *P. asparagi* infection

In the middle and late stages of infection, we used SEM and CLSM to observe the surface and intracellular hyphae of the stem. We found that a large number of conidia on the host surface couldn't germinate, which eventually shrank and died. Only less than 10% of them were able to successfully germinate after 3 dpi (Fig. 7a, e). At 5 dpi, almost no hyphae were found on the host surface. Occasionally, a few residual hyphae were surrounded by callose-like substances (Fig. 7b–d). In the stem center, clear and intact cellular outlines could be stained by PI at 11 dpi (Fig. 7f), indicating that asparagus stem cells may be alive at this stage even after the extensive proliferation of *P. asparagi* inside them. By PI staining, we observed a few dead invasive hyphae at this stage. At 13 dpi, the clear and intact cellular outlines of the asparagus stem cortical tissue cells were not able to be seen, where more dead invasive hyphae were also be observed by PI staining (Fig. 7g).

The temporal-spatial accumulation of H₂O₂ during pathogen infection

During the fungal colonization, intracellular H₂O₂ production was analyzed using the corresponding

fluorescent probes. Compared to the basal level of H₂O₂ in uninfected stems (Fig. 8a, d), the penetration of hyphae led to a rapid generation and release of H₂O₂ in both the epidermis and vascular system after 1 day of inoculation. The accumulation of H₂O₂ culminated at its peak concentration at 3 dpi, and then decreased markedly (Fig. 8c, d). At 5 dpi, H₂O₂ mainly were distributed in the epidermis and vascular bundles. However, at 7 dpi, when hyphae reached the cortex (Fig. 8b), H₂O₂ accumulation was seen throughout the parenchyma cells in the entire stem. At 11 dpi and 13 dpi, very little H₂O₂ was produced in the epidermis and vascular system (Fig. 8c), less than that at 1dpi (Fig. 8d).

Discussion

Pathogenic fungi frequently employ specialized infection structures, such as appressorium or infection cushions, to facilitate their invasion on host plants. For example, the rice blast pathogen *M. r. oryzae* achieves entry into host cells through mechanical penetration of the cuticle, accomplished by the formation of a dome-shaped and melanized appressorium (Howard and Valent 1996). Similarly, *F. graminearum*, the fusarium head blight (FHB) in cereals, and *B. cinerea*, the grey mold disease, penetrate plants by means of infection cushions (Mentges et al. 2020; Choquer et al. 2021). In the present study, the utilization of SEM revealed that *P. asparagi* mainly exhibited two specialized morphological structures, the appressoria and penetration pegs, which substantially facilitate colonization. Furthermore, the conidia and hyphae of *P.*

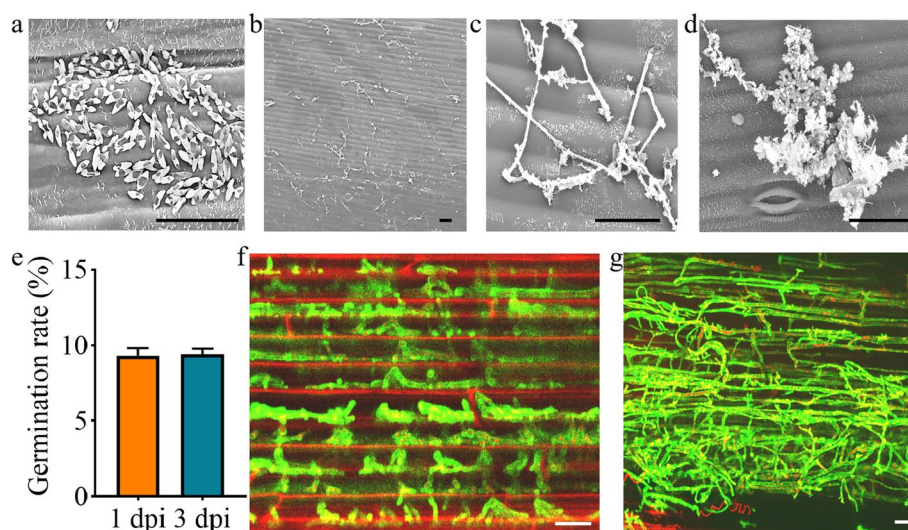


Fig. 7 Observation of defense response in the host stem surface and in tissues. **a** Conidia cannot germinate that had eventually shrank on the stem (3 dpi) ($n = 1000$, three independently repeated experiments). **b**, **c**, and **d** Stem surface hyphal were surrounded by the callose-like substances (amorphous material) (11 dpi). **e** Statistics assays of conidia germination rates at 1 and 3 dpi. **f** The cell wall of stem tissue and a few hyphae were stained by PI at 11 dpi. **g** The content of the infected epidermic cells was disintegrated by PI staining at 13 dpi. Scale bars: 30 μ m

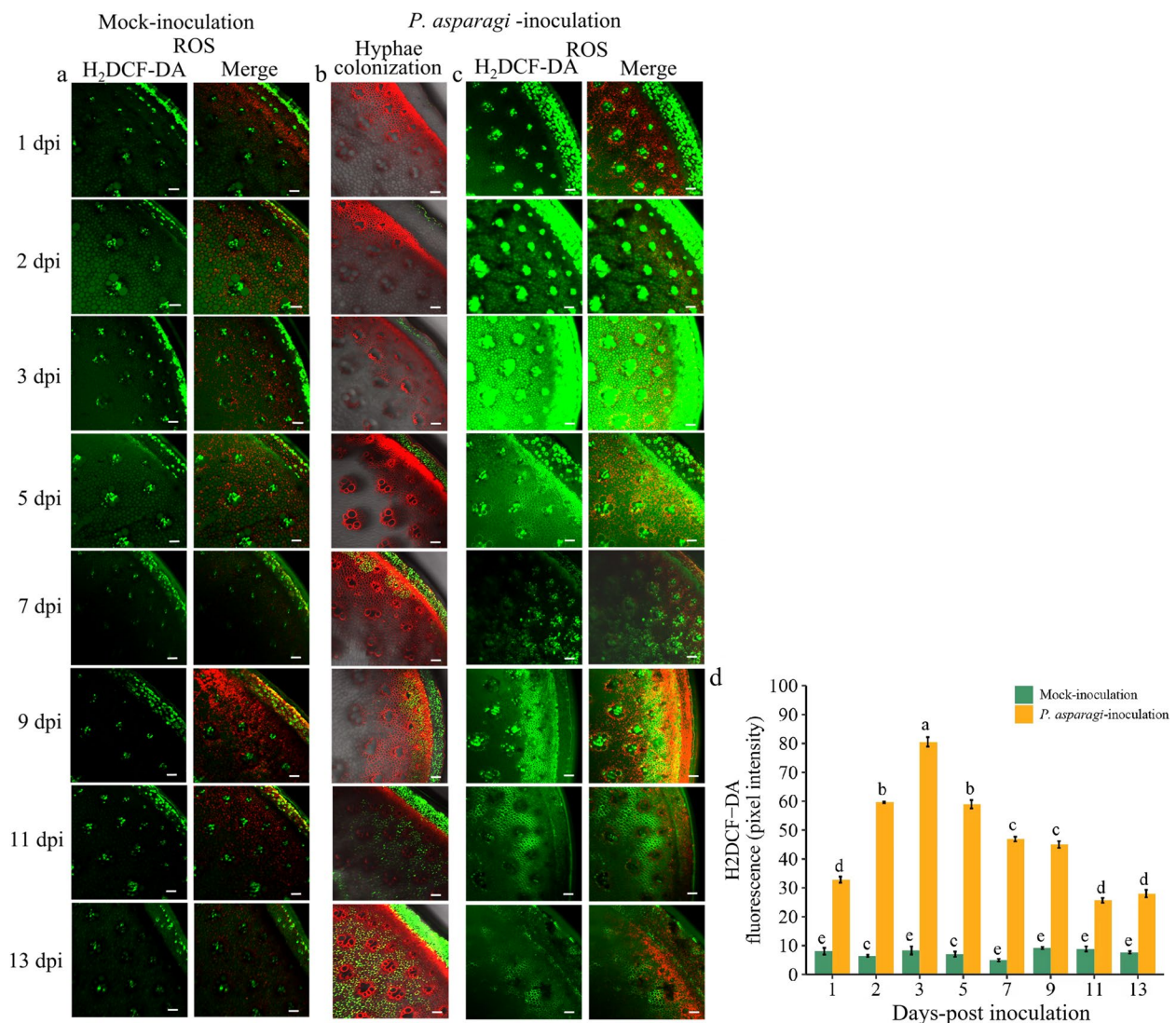


Fig. 8 H_2O_2 accumulation and location by a time-course observation in the plants infected by *P. asparagi*. **a** H_2O_2 fluorescence images for mock-treated samples. **b** *P. asparagi* colonization in the stem tissues. **c** H_2O_2 fluorescence images for infected stems. ROS was stained with H₂DCF-DA (green fluorescence); Chlorophyll showed red autofluorescence. Fungal cells were stained with WGA-AF488 (green fluorescence), and the plant cell wall was stained with PI (red fluorescence). Scale bars: 100 μ m. **d** Quantification of the H₂DCF-DA fluorescence intensities in **a** and **c**. Data from three biological replicates were analyzed by Student's t-test. Different letters indicate significant differences ($P \leq 0.01$)

asparagi were found to secrete mucilaginous substances on the host surface, potentially contributing to their survival and dispersal. Notably, apart from the penetration pore, no clear damage was observed in these tissues, indicating that it necessitates further investigation for the underlying mechanism in host penetration. Additionally, it was observed that certain pathogen hyphae were capable of invading host tissues through stomata without any discernible morphological alterations (Steinberg 2015; Yin et al. 2017). In our study, we observed fungal penetration exclusively through the epidermis, with rare instances of penetration through the opening stomata,

suggesting that stomata do not serve as the primary pathway for infection. This finding aligns with previous research on *M. oryzae* and *Exserohilum turcicum*, which suggests that stomata may not contribute to the entry of these pathogens (Minker et al. 2018; Kotze et al. 2019; Qiu et al. 2019).

The macroscopic symptoms observed in asparagus stem after pathogen inoculation are consistent with those observed in the field and previous studies (Yang et al. 2016). Symptoms were observed to manifest at 3–5 dpi, with a larger area affected at 7–9 dpi. The stem displayed withering, and numerous small black pycnidia, which

were scattered throughout the affected region within 12–14 days. Microscopic examination revealed that the fungal hyphae penetrated the plant surface within 1 day of inoculation, and reached the sclerenchyma sheath cells at 2 dpi. They subsequently formed sporodochia at 7–9 dpi. Furthermore, the hyphae exhibited extensive spreading, resulting in severe stem blight at 7 dpi, and conidia were released at 14–16 dpi. Prior to 5 dpi, the majority of hyphae were confined to the epidermis. However, during the middle and late stages of infection, there was a rapid expansion of hyphae within the tissue, leading to an acceleration of stem wilting. This result may be attributed to the inhibition of expansion by epidermal cells and the dense sclerenchyma sheath cells.

Through ultrastructural investigations, we found that the infection sites exhibited fungi proliferation and divergence, resulting in rapid dissemination of both inter- and intracellular hyphae. In this study, the inherent haustoria were not observed at the *P. asparagi*-asparagus stem interface. Haustoria, which are specialized feeding structures formed by biotrophic fungi or oomycetes, serve as a means for these pathogens to acquire nutrients from their hosts (Slusarenko and Schlaich 2003; Yi and Valent 2013). The mechanism by which the pathogen obtains nutrition from the host remains unclear. Notably, the process of cell-to-cell movement of the hyphae, characterized by initial swelling followed by extreme constriction, bears a resemblance to the formation of an appressorium penetration peg. Both structures exhibit similar diameters when examined by SEM, suggesting that *P. asparagi* exhibited biotrophic growth by penetrating the epidermal walls and cell-to-cell movement by a flexible invasion peg, which is commonly observed in biotrophic pathogens. These results align with previous studies for rice blast disease and FHB (Kankanala et al. 2007; Qiu et al. 2019). The swelling structure observed in the hyphal tip is likely a result of cytoplasm accumulation in response to the mechanical resistance of the plant tissue (Eynck et al. 2007). However, the mechanism underlying cell-to-cell invasion requires further investigation.

Pathogen secreted effector triggered plant immune responses are typically accompanied by cell death resulting from hypersensitive responses (HR) (Pitsili et al. 2020; Yin et al. 2022). Localized cell death is employed by plants to impede the dissemination of pathogens, and mitochondria are associated with HR (Lam et al. 2001; Ordog et al. 2002). In this study, TEM analysis unveiled that a majority of epidermal cells displayed plasmolysis at 3 dpi. Additionally, electron-dense precipitates were observed to accumulate around the cell membrane, accompanied by cell wall collapse or complete disappearance, as well as organelle destruction, particularly the mitochondria. This observation suggests that local cell

death within the epidermis could potentially contribute to disease resistance. Furthermore, it is plausible that the cell wall-degrading enzymes produced by these pathogens contribute to the degradation of the host's cell wall, which facilitated the infected cell death.

The germination time of *P. asparagi* is consistent with that of the culture medium. However, there is a notable disparity in the germination rate. Some conidia germinate and a few hyphae successfully penetrate the surface of the host stem. This phenomenon may be attributed to the resistance of host stem, which inhibits conidia germination and hyphae invasion. The production of callose-like substance serves as an indication of plant defense responses. The PI staining was observed during later stages of infection, suggesting the death of hyphae. Comparable findings have been reported in wheat coleoptiles infected with *F. graminearum*, where hyphae vacuolization was also observed (Minker et al. 2018), although no vacuolated hyphae were observed in *P. asparagi*.

Pathogen infection process is heavily influenced by the dynamic fluctuations in ROS (Sang and Macho 2017). Our findings demonstrate a notable increase in H_2O_2 levels during the later stages of infection, commencing at spore germination and persisting until the penetration on the epidermis. Moreover, at 3 dpi, the accumulation of H_2O_2 is significantly higher, aligning with the manifestation of necrotic symptoms. This heightened presence of H_2O_2 may be attributed to a hypersensitive response in plants, which restricts the dissemination of pathogens by inducing mitochondrial and chloroplast dysfunction, and ultimately leads to cell death. ROS serves as highly conserved intercellular stress signals, and in vascular plants, long-distance communication occurs via the vascular system (Fichman et al. 2023). Additionally, the death of the fungal pathogens can be induced by H_2O_2 (Qin et al. 2011). In the case of *P. asparagi* infection, elevated levels of H_2O_2 were observed in the epidermal cells in asparagus stems. The production and concentration of H_2O_2 in the vascular bundle are particularly higher, and the entry of hyphae into the vascular bundle is rare. These findings indicate that H_2O_2 primarily contributes to the resistance of *P. asparagi* infection.

Conclusion

Through the utilization of contemporary microscopy technology, a comprehensive examination of the complete infection process of *P. asparagi* suggests that it effectively infiltrates asparagus stems by means of appressoria-like structures or narrow pegs. The movement of hyphae between cells is facilitated by the presence of constricted invasive hyphae pegs, which extend along the inner side of the cell wall and towards the central cylinder. The host's defense mechanisms encompass

the production of callose analogs and the initiation of oxidative bursts. These findings provide new insights into the infection process and host response characteristics during interactions between *P. asparagi* and asparagus, thereby contributing valuable knowledge towards a more comprehensive understanding of *P. asparagi* pathogenesis.

Methods

Plant material

Four-year-old plants of asparagus variety 'Feicuiming-zhu' were cultivated in pots with a diameter of 50 cm in a greenhouse. The plants were grown under a 14-hour light and 10-hour dark-light cycle, and temperatures ranged from 20 to 25°C, with the relative humidity between 40 and 60%, and a light intensity of 60 mE/s/m². When the plants reached a height of 6–8 cm, the stems were used for fungus inoculation.

Fungi isolation and identification

The causal fungus *P. asparagi* was isolated from a diseased asparagus stem that displayed typical symptoms of stem blight in an asparagus plant. A diseased stem is cleaned and sterilized with 70% ethanol, then a sterilized knife is used to cut the stem longitudinally, and take a small area of diseased tissue culturing on potato sucrose agar (PSA) medium (potato 200 g, sucrose 20 g, agar 18 g, and ddH₂O 1000 mL), followed by the subculturing purification. The identity of the causal pathogen was primarily confirmed by traditionally morphological identification, including the characteristics in medium and conidia, hyphae morphological and pathogenicity assay. For further identification, the molecular identification by amplifying and sequencing its rDNA internal transcribed spacer (ITS). The target band was purified and sequenced in both directions using fungi amplification universal primers (ITS1: 5'-TCCGTAGGTGAACCTGCGG-3'; ITS4: 5'-TCCTCCGCTTATTGATATGC-3'), and the resulting sequences were blasted with the gene sequence in GeneBank database.

Pathogen inoculation

The isolated *P. asparagi* was cultured with PSA medium at 25°C under a 12-hour photoperiod. After 12–14 days of incubation, when the pycnidia were produced, the conidia were washed out of the pycnidia using sterile water, which was then filtered through double-layer sterile lens cleaning paper and counted with a hemocytometer under 40× magnification. The spore suspension for inoculations was adjusted to 1 × 10⁷ spores/mL with sterile water.

Asparagus plants were inoculated with spores of *P. asparagi* with adjusted concentration using the vinyl

cotton (VC) method (Sonoda et al. 1997) with minor modifications. The basal part of the tender stem was wrapped in 1 cm × 1 cm cotton strips, then 1.0 mL of *P. asparagi* inoculum was infiltrated gently into the cotton with a Pasteur pipette, and incubated in a growth chamber at 25°C and 90% humidity for 3 days. Plants treated with sterile distilled water under the same conditions were used as a control. The incubated plants were then transferred to a glasshouse at 25 ± 1°C under natural daylight. The disease symptoms were observed, and the inoculated stem tissues were harvested at each time point after infection for microscopic observations. The experiments were performed three times independently, and at least three stems were analyzed at each time point.

Observation of stem blight symptoms

The phenotypic alterations in the stem surface after the inoculation with *P. asparagi* were recorded using photography. The severity of the disease was assessed by employing a grading system based on the proportion of the stem area affected by lesions. 0 = No symptoms, 1 = 1 to 10% covered with lesion, 2 = 11 to 30% covered with lesions, 3 = 31 to 50% covered with lesion, 4 = 50 to 75% blights and 5 = 75 to 100% blights and plants dead.

Scanning electron microscopy observation

To observe the surface structure of fungal colonization and proliferation, we used SEM to observe the stem surface and cross sections of infected asparagus stems. The samples were fixed in a formalin-alcohol-acetic acid (FAA, 90:5:5) solution at 4°C overnight and dehydrated in an ethanol series (50%, 70%, 80%, 90%, and twice in 100% ethanol) for 25 min per concentration. Then, they were rinsed two times in tert-butanol to replace ethanol and dried for 1–3 h. Finally, the samples were sputter coated with gold particles and observed with an S-3000 N scanning electron microscope (Hitachi, Japan).

Confocal microscopy observation

The samples were hand-cut into 60 μm thick sections and bleached with pure ethanol. They were then incubated in 10% KOH for 2–3 h at 85°C, which were further neutralized with five washing steps using phosphate-buffered saline (PBS) at pH 7.4. Subsequently, the sliced samples were stained with WGA-AF488 (catalog No. W11261, Thermo Fisher Scientific) and propidium iodide (PI) (catalog No. P4170, Sigma-Aldrich) (1 μg/mL PI, 10 μg/mL WGA-AF488; 0.02% Tween-20 in PBS, pH 7.4). Confocal images were taken by a TCS-SP8 confocal microscope (Leica, Germany). WGA-AF 488 was used to stain fungal cell walls as green using excitation at 488 nm and detection at 500–540 nm, and PI was used to stain plant cell

walls as red using excitation and emission at 543 nm and 560–615 nm, respectively (Redkar et al. 2018).

Transmission electron microscope observation

The epidermis from inoculated stems at 3 dpi and mock were prepared using a razor blade to excise approximately 1 mm³ pieces. These pieces were immediately fixed in 2.5% glutaraldehyde (pH 7.4) for 2 h. The samples were then washed three times with 0.1 M phosphate buffer (pH 7.2) and fixed in 1% osmic acid at 4°C for 2 h. After washes, the samples were dehydrated in a graded series of ethanol, embedded in Epon-Araldite resin for penetration, and placed in a mold for polymerization. After the semi-thin sections were used for positioning, the ultrathin sections were made and collected. The sections were counterstained with 3% uranyl acetate and 2.7% lead citrate and were observed with a JEM1400 transmission electron microscope (JEOL, Japan).

Reactive oxygen species (ROS) detection

H₂O₂ production and location were detected in the entire infection cycle using the H₂DCF-DA staining method (Kaur et al. 2016; Zhao et al. 2020). Transection samples were incubated in 10 μM H₂DCF-DA (catalog No.4,610,273, Sigma-Aldrich) for 10 min at room temperature, then they were washed three times with 100 mM PBS (pH 7.4) to remove excess H₂DCF-DA. Fluorescence was detected with a confocal laser scanning microscope (Leica, Germany) using the following settings: 70% power, excitation at 488 nm, and emission at 505 to 530 nm. This experiment was independently repeated at least three times.

Statistical analysis

The disease indexes and ratio of lesion area were quantified by lesion or hyphae growth area to the total area, and H₂DCF-DA fluorescence intensities were quantified using Image J. Results represent the means of three replicate stems, and the data are presented as means ± standard deviation (SD). Different letters indicate significant differences between the samples at $P < 0.01$. Significant differences between groups were determined using independent-samples Student's *t*-test and one-way ANOVA with GraphPad software (version 8.0.2).

Abbreviations

3D	Three dimension
CLSM	Confocal laser scanning microscope
dpi	Days post inoculation
FHB	Fusarium head blight
H ₂ O ₂	Hydrogen peroxide
hpi	Hours post inoculation
HR	Hypersensitive responses
ITS	Internal transcribed spacer
PBS	Phosphate-buffered saline
PI	Propidium iodide

ROS	Reactive oxygen species
SD	Standard deviation
SEM	Scanning electron microscopy
TEM	Transmission electron microscope
VC	Vinyl cotton

Supplementary Information

The online version contains supplementary material available at <https://doi.org/10.1186/s42483-024-00252-x>.

Additional file 1: Video S1. *P. asparagi* pycnidium forming beneath the epidermis.

Additional file 2: Video S2. The proliferation of *P. asparagi* hyphae in the tissue.

Additional file 3: Video S3. *P. asparagi* invasive hyphae cell-to-cell movement.

Acknowledgements

Not applicable.

Authors' contributions

LS performed the investigation, writing-original draft, writing-review, and editing. YL, XL, XR, YZ, RW, SW, NC, and YZ performed investigation and formal analysis. SL conducted conceptualization, writing, review, and editing. WG performed conceptualization, writing, review, and editing.

Funding

This work was supported by grants from the National Natural Science Foundation of China (31970240 and 32170336), the National Science Foundation of Henan Province (222300420053), and the Program for Science & Technology Innovation Talents in the Universities of Henan Province (23HASTIT035).

Availability of data and materials

Data will be made available on request.

Declarations

Ethics approval and consent to participate

Not applicable.

Consent for publication

Not applicable.

Competing interests

The authors declare that they have no competing financial interests or personal relationships that could have appeared to influence the work reported in this paper.

Received: 15 January 2024 Accepted: 6 May 2024

Published online: 04 July 2024

References

- Ali S, Ganai BA, Kamili AN, Bhat AA, Mir ZA, Bhat JA, Tyagi A, Islam ST, Mushtaq M, Yadav P. Pathogenesis-related proteins and peptides as promising tools for engineering plants with multiple stress tolerance. *Microbiol Res.* 2018;212:29–37. <https://doi.org/10.1016/j.micres.2018.04.008>.
- Bolwell GP. Role of active oxygen species and NO in plant defence responses. *Curr Opin Plant Biol.* 1999;2:287–94. [https://doi.org/10.1016/S1369-5266\(99\)80051-X](https://doi.org/10.1016/S1369-5266(99)80051-X).
- Choquer M, Rasclé C, Gonçalves IR, de Vallée A, Ribot C, Loisel E, Smilevski P, Ferria J, Savadogo M, Souibgui E. The infection cushion of *Botrytis Cinerea*: a fungal 'weapon' of plant-biomass destruction. *Environ Microbiol.* 2021;23:2293–314. <https://doi.org/10.1111/1462-2920.15416>.

- Davis RD. Asparagus stem blight recorded in Australia. *Australas Plant Path.* 2001;30:181–2. <https://doi.org/10.1071/AP01022>.
- Elena K. First report of *Phomopsis asparagi* causing stem blight of asparagus in Greece. *Plant Pathol.* 2006;55:300. <https://doi.org/10.1111/j.1365-3059.2005.01265.x>.
- Eynck C, Koopmann B, Grunewaldt-Stoecker G, Karlovsky P, Von Tiedemann A. Differential interactions of *Verticillium Longisporum* and *V. dahliae* with *Brassica napus* detected with molecular and histological techniques. *Eur J Plant Pathol.* 2007;118:259–74. <https://doi.org/10.1007/s10658-007-9144-6>.
- Fichman Y, Rowland L, Oliver MJ, Mittler R. ROS are evolutionary conserved cell-to-cell stress signals. *PNAS.* 2023;120(31):e2305496120. <https://doi.org/10.1073/pnas.2305496120>.
- Fincher GB. Engineering disease resistance in crop plants: callosic papillae as potential targets. *Engineering.* 2020;6:505–8. <https://doi.org/10.1016/j.eng.2020.03.012>.
- Howard RJ, Valent B. Breaking and entering: host penetration by the fungal rice blast pathogen *Magnaporthe Grisea*. *Annu Rev Microbiol.* 1996;50:491–512. <https://doi.org/10.1146/annurev.micro.50.1.491>.
- Iwato M, Kosaza M, Takeuchi Y, Matsumoto M, Inada M. Stem blight resistance of *Asparagus kiusianus* and its hybrid with *A. Officinalis*. *Adv Hort Sci.* 2014;28:202–7. <http://digital.casalini.it/10.1400/230469>.
- Kankanala P, Czymmek K, Valent B. Roles for rice membrane dynamics and plasmodesmata during biotrophic invasion by the blast fungus. *Plant Cell.* 2007;19:706–24. <https://doi.org/10.1105/tpc.106.046300>.
- Kasprzewska A. Plant chitinases-regulation and function. *Cell Mol Biol Lett.* 2003;8:809–24 PMID: 12949620.
- Kaur N, Sharma I, Kirat K, Pati PK. Detection of reactive oxygen species in *Oryza sativa* L. (rice). *Bio-protocol.* 2016;6:e2061–e2061. <https://doi.org/10.21769/BioProtoc.2061>.
- Kotze RG, Van der Merwe CF, Crampton BG, Kritzing Q. A histological assessment of the infection strategy of *Exserohilum turcicum* in maize. *Plant Pathol.* 2019;68:504–12. <https://doi.org/10.1111/ppa.12961>.
- Lam E, Kato N, Lawton M. Programmed cell death, mitochondria and the plant hypersensitive response. *Nature.* 2001;411:848–53. <https://doi.org/10.1038/35081184>.
- McKirdy S, Murphy P, Mackie AE, Kumar S. Survey of asparagus in Western Australia for rust and stem blight. *Australas Plant Path.* 2002;31:97–8. <https://doi.org/10.1071/AP01073>.
- Mentges M, Glasenapp A, Boenisch M, Malz S, Henrissat B, Frandsen RJ, Güldener U, Münsterkötter M, Bormann J, Lebrun MH. Infection cushions of *Fusarium graminearum* are fungal arsenals for wheat infection. *Mol Plant Pathol.* 2020;21:1070–87. <https://doi.org/10.1111/mpp.12960>.
- Minker KR, Biedrzycki ML, Kolagunda A, Rhein S, Perina FJ, Jacobs SS, Moore M, Jamann TM, Yang Q, Nelson R. Semiautomated confocal imaging of fungal pathogenesis on plants: microscopic analysis of macroscopic specimens. *Microsc Res Techniq.* 2018;81:141–52. <https://doi.org/10.1002/jemt.22709>.
- Moosa A, Farzand A, Sahi ST, Khan SA. Transgenic expression of antifungal pathogenesis-related proteins against phytopathogenic fungi—15 years of success. *Isr J Plant Sci.* 2018;65:38–54. <https://doi.org/10.1080/07929978.2017.1288407>.
- Ordog SH, Higgins VJ, Vanlerberghe GC. Mitochondrial alternative oxidase is not a critical component of plant viral resistance but may play a role in the hypersensitive response. *Plant Physiol.* 2002;129:1858–65. <https://doi.org/10.1104/pp.003855>.
- Pitsili E, Phukan UJ, Coll NS. Cell death in plant immunity. *CSH Perspect Biol.* 2020;12:a036483. <https://doi.org/10.1101/cshperspect.a036483>.
- Qin G, Liu J, Cao B, Li B, Tian S. Hydrogen peroxide acts on sensitive mitochondrial proteins to induce death of a fungal pathogen revealed by proteomic analysis. *PLoS ONE.* 2011;6:e21945. <https://doi.org/10.1371/journal.pone.0021945>.
- Qiu H, Zhao X, Fang WQ, Wu HM, Abubakar YS, Lu GD, Wang ZH, Zheng WH. Spatiotemporal nature of *Fusarium graminearum*-wheat coleoptile interactions. *Phytopathol Res.* 2019;1:1–12. <https://doi.org/10.1186/s42483-019-0033-7>.
- Redkar A, Jaeger E, Doehlemann G. Visualization of growth and morphology of fungal hyphae in planta using WGA-AF488 and propidium iodide co-staining. *Bio-protocol.* 2018. <https://doi.org/10.21769/BioProtoc.2942.e2942>.
- Roulin S, Xu P, Brown AH, Fincher GB. Expression of specific (1→3)-β-glucanase genes in leaves of near-isogenic resistant and susceptible barley lines infected with the leaf scald fungus (*Rhynchosporium Secalis*). *Physiol Mol Plant P.* 1997;50:245–61. <https://doi.org/10.1006/pmpp.1997.0084>.
- Sang YP, Macho AP. Analysis of PAMP-triggered ROS burst in plant immunity. *Plant pattern recognition receptors: methods and protocols.* 2017:143–153. https://doi.org/10.1007/978-1-4939-6859-6_11.
- Slusarenko AJ, Schlaich NL. Downy mildew of *Arabidopsis thaliana* caused by *Hyaloperonospora Parasitica* (formerly *Peronospora Parasitica*). *Mol. Plant Pathol.* 2003;4:159–70. <https://doi.org/10.1046/j.1364-3703.2003.00166.x>.
- Sonoda T, Uragami A, Kaji K. Evaluation of *Asparagus officinalis* cultivars for resistance to stem blight by using a novel inoculation method. *HortScience.* 1997;32:1085–6. <https://doi.org/10.21273/HORTSCI.32.6.1085>.
- Steinberg G. Cell biology of *Zymoseptoria Tritici*: Pathogen cell organization and wheat infection. *Fungal Genet Biol.* 2015;79:17–23. <https://doi.org/10.1016/j.fgb.2015.04.002>.
- Takeuchi Y, Kakizoe E, Yoritomi R, Iwato M, Kanno A, Ikeuchi T, Mori M, Murakami K, Uragami A, Matsumoto M. Features in stem blight resistance confirmed in interspecific hybrids of *Asparagus officinalis* L. and *Asparagus Kiusianus* Makino. *Horticult. J.* 2018;87:200–5. <https://doi.org/10.2503/hortj.OKD-104>.
- Talbot NJ. On the trail of a cereal killer: exploring the biology of *Magnaporthe Grisea*. *Annu Rev Microbiol.* 2003;57:177–202. <https://doi.org/10.1146/annurev.micro.57.030502.090957>.
- Thao L, Dung N. First report of *Phomopsis asparagi* causing stem blight on asparagus in Vietnam. *New Disease Rep.* 2019;39:7–7. <https://doi.org/10.5197/j.2044-0588.2019.039.007>.
- Uecker F, Johnson DA. Morphology and taxonomy of species of *Phomopsis* on Asparagus. *Mycologia.* 1991;83:192–9. <https://doi.org/10.1080/00275514.1991.12025995>.
- Van Baarlen P, Staats M, Van Kan JA. Induction of programmed cell death in lily by the fungal pathogen *Botrytis Elliptica*. *Mol Plant Pathol.* 2004;5:559–74. <https://doi.org/10.1111/j.1364-3703.2004.00253.x>.
- Wojtaszek P. Oxidative burst: an early plant response to pathogen infection. *Biochem J.* 1997;322:681–92. <https://doi.org/10.1042/bj3220681>.
- Yang YQ, Sun Q, Li CM, Chen HF, Zhao F, Huang JH, Li XM, Lan B. Identification of the pathogen of asparagus stem blight and analysis of its regional difference. In XIII International Asparagus Symposium. 2012; 185–192. <https://doi.org/10.17660/ActaHortic.2020.1301.29>.
- Yang YQ, Lan B, Jian YL, Chang DD, Zhang SL, Li XM. Infection process and pathogenic mechanism of *Phomopsis asparagi*, the Asparagus stem blight pathogen. *Phytoparasitica.* 2016;44:11–8. <https://doi.org/10.1007/s12600-015-0499-5>.
- Yang YQ, Sun Q, Li CM, Chen HF, Zhao F, Huang JH, Zhou JM, Li XM, Lan B. Biological characteristics and genetic diversity of *Phomopsis asparagi*, causal agent of asparagus stem blight. *Plant Dis.* 2020;104:2898–904. <https://doi.org/10.1094/PDIS-07-19-1484-RE>.
- Yi M, Valent B. Communication between filamentous pathogens and plants at the biotrophic interface. *Annu Rev Phytopathol.* 2013;51:587–611. <https://doi.org/10.1146/annurev-phyto-081211-172916>.
- Yin X, Liu RQ, Su H, Su L, Guo YR, Wang ZJ, Du W, Li MJ, Zhang X, Wang YJ. Pathogen development and host responses to *Plasmopara Viticola* in resistant and susceptible grapevines: an ultrastructural study. *Hortic Res.* 2017;4:1–10. <https://doi.org/10.1038/hortres.2017.33>.
- Yin JJ, Xiong J, Xu LT, Chen XW, Li WT. Recent advances in plant immunity with cell death: a review. *J Integr Agr.* 2022;21:610–20. [https://doi.org/10.1016/s2095-3119\(21\)63728-0](https://doi.org/10.1016/s2095-3119(21)63728-0).
- Zaw M, Naing T, Matsumoto M. First report of stem blight of asparagus caused by *Phomopsis asparagi* in Myanmar. *New Disease Rep.* 2017;35:17. <https://doi.org/10.5197/j.2044-0588.2017.035.017>.
- Zhang Y, Araki H. Production Trend and Cropping System of Asparagus in China. *Japanese J Farm Work Res.* 2017;52:27–35. <https://doi.org/10.4035/jsfwr.52.27>.
- Zhao J, Chen QH, Zhou S, Sun YH, Li XY, Li YZ. H2Bub1 regulates RbohD-dependent hydrogen peroxide signal pathway in the defense responses to *Verticillium Dahliae* toxins. *Plant Physiol.* 2020;182:640–57. <https://doi.org/10.1104/pp.19.00913>.
- Zheng JL, He CP, Yi KX, Xi JG, Gao JM, Zhang SQ, et al. Research progress on asparagus stem wilt and disease resistance breeding. *Chin J Tropical Agric.* 2015;35:65–70. <http://doi.org/CNKI:SN:RNDK.0.2015-11-013>.